Lens stars and Platonic lenses

JAKUB BĚLÍN,[1,2,*] **JOHANNES COURTIAL,**[2] **AND TOMÁŠ TYC**[3]

[1]*Central European Institute of Technology, Brno University of Technology, Purkyňova 656/123, 612 00 Brno, Czech Republic*
[2]*School of Physics & Astronomy, College of Science & Engineering, University of Glasgow, Glasgow G12 8QQ, United Kingdom*
[3]*Institute of Theoretical Physics and Astrophysics, Faculty of Science, Masaryk University, Kotlářská 2, 61137 Brno, Czech Republic*
*jakub.belin@ceitec.vutbr.cz

Abstract: Lens stars comprise identical ideal thin lenses arranged in a regular star shape centred on the common principal point. They satisfy the edge-imaging condition of transformation optics (TO) and are thus suitable as building blocks of ideal-lens TO devices [J. Opt. Soc. Am. A **37**, 305 (2020)]. Here we show that the ray trajectories in lens stars are piecewise straight approximations of conic sections. We also generalise lens stars to Platonic lenses, highly symmetric combinations of lens stars based on Platonic solids, and find that ray trajectories in Platonic lenses are closed and planar; we design a more general ideal-lens cloak; and we clarify the process of designing ideal-lens TO devices. Throughout, we illustrate our results with ray-tracing simulations. Our results add to the knowledge of TO with ideal lenses.

1. Introduction

Transformation optics (TO) [1,2] is a highly active field of research. In a nutshell, TO applies the mathematics of differential geometry to fabricate material structures and devices that distort the trajectories of light rays passing through. As a result, such devices change the apparent shape and/or size of any object inside it. The actual structure is said to be in physical space, whereas the apparent structure as seen from the outside is said to be in a virtual space. The ideas of TO already penetrated to other branches of physics, resulting, for example, in optical simulations of curved space-times [3,4], transformation thermodynamics [5,6], acoustic cloaking [7], elastic cloaking [8], and seismic cloaking [9]. To realise the devices proposed by TO in practice, highly advanced material engineering is usually required and some designs can not be realised at all [10]. Due to these limitations, several research groups started to construct TO devices from naturally occurring crystals [11–14] or from lenses [15–17].

In recent work [18,19], we have presented a theory of building omnidirectional TO devices using ideal thin lenses and applied that theory to design an omnidirectional lens, an ideal-lens structure that can also function as a cloak. Our method of designing ideal-lens TO devices is based on identity-mapping conditions on certain combinations of lenses, requiring each lens combination to image any object position back to itself. Specifically, we have formulated the *loop-imaging condition*: the combination of any lenses (and, more generally, other optical components) encountered along any closed loop in a TO device must image any object point to itself. Here, the closed loop is meant to be a notional path, not a light-ray trajectory. The imaging due to the lenses encountered along such a notional loop is then supposed to be performed in a direction given by the loop and leads to closed light-ray trajectories only if the considered lens combination images any object point back to itself. To recognize whether a lens structure is a TO device or not, we have formulated the *loop-imaging theorem*: in a TO device, the loop-imaging condition is satisfied for every closed loop in the structure. Thankfully, it is not necessary to test the loop-imaging condition for every closed loop in a lens structure: it turns out that it is

sufficient to test the loop-imaging condition only for those loops around edges in the structure where several lenses meet. We call this stronger condition the *edge-imaging condition* [17].

Employing the edge-imaging condition, we derived rules for the placement of the principal points and started building up a "library" of lens-based building blocks for TO devices by applying the edge-imaging condition to different combinations of lenses [20]. The results allow quick and easy selection of suitable TO designs and calculation of all lens parameters. One of the "building blocks" presented in Ref. [20] is the so-called "lens star": a combination of ideal thin lenses, all with the same focal length and the same principal point, which is positioned on the single straight line along which all lenses intersect, and with identical angles between neighbouring lenses. Lens stars satisfy the loop-imaging condition for any loop that surrounds the single intersection line.

Here we further develop the theory of lens stars. We introduce continuous lens stars and with their help we analyse ray propagation in lens stars. In particular, we show that light-ray trajectories in lens stars are tightly related to conic sections, and analyse collimation effect of lens stars. Finally, we generalise lens stars to highly symmetric 3D structures of lenses based on Platonic solids, which we call *Platonic lenses*, and present raytracing simulations of the view through and from within these structures.

2. Imaging due to a lens star

We define a regular lens star as a structure of N ideal thin lenses $L_1, \ldots, L_N$ with a common focal length f, intersecting in a common edge, the *star axis*, such that their principal points coincide and the angles between two neighbouring lenses are the same. An example of a lens star for $N = 5$ is shown in Fig. 1(a). To prove that such defined lens star satisfies the edge-imaging condition, we will derive the imaging equation due to n lenses of the star (where $n \leq N$ is chosen arbitrarily) and show that for $n = N$ the object and image positions coincide.

An ideal thin lens is a theoretical device consisting of a planar surface that bends light rays on transmission (without offsetting them) such that it images stigmatically (i.e., point-to-point) any object point $\mathbf{O} = (x, y, z)$ to a corresponding image point $\mathbf{I} = (x', y', z')$. If the coordinate system is chosen such that its origin coincides with the lens's principal point (i.e., the point through which the light rays propagate unaffected) and the z axis coincides with the optical axis (i.e., the axis through the principal point perpendicular to the lens), the object and image positions are related by the ideal-lens imaging equations [21]

$$-\frac{1}{z} + \frac{1}{z'} = \frac{1}{f}, \quad \frac{x'}{x} = \frac{y'}{y} = \frac{z'}{z},$$ (1)

where f is the lens's focal length. This corresponds to a law of refraction $\theta' = \theta - r/f$, where θ and θ' are direction cosines of the incident and the transmitted light ray respectively, and r is a distance between the point where the light ray intersects the lens and its principal point [22].

The derivation of the imaging equation of a lens star is based on the following idea: when a lens produces an image of an arbitrary object point O, that image is located on the straight line through the object point and the lens' principal point P. Because the centre of the lens star is the principal point of all lenses in the star, any object and its images produced by successive lenses lie on a single *image line*: the straight line through the centre P of the star (depicted as *o*-axis in Fig. 2). We denote $\hat{\mathbf{o}}$ the unit vector parallel to the image line.

Now, we will find the image I_n of an arbitrary object point O due to $n \leq N$ lenses in the star. It is instructive to first describe imaging due to a single lens L_k of the star. This lens provides an image I_k of point I_{k-1} that corresponds to the intermediate image of O due to $k - 1$ lenses prior to L_k. To describe the image position, we will use vector notation where $\mathbf{A}$ denotes the radius vector of point A with respect to the principal point P which we place to the origin of coordinates. Using the vector form of the ideal-lens imaging Eq. (1) (easily derived from Eq. (4)
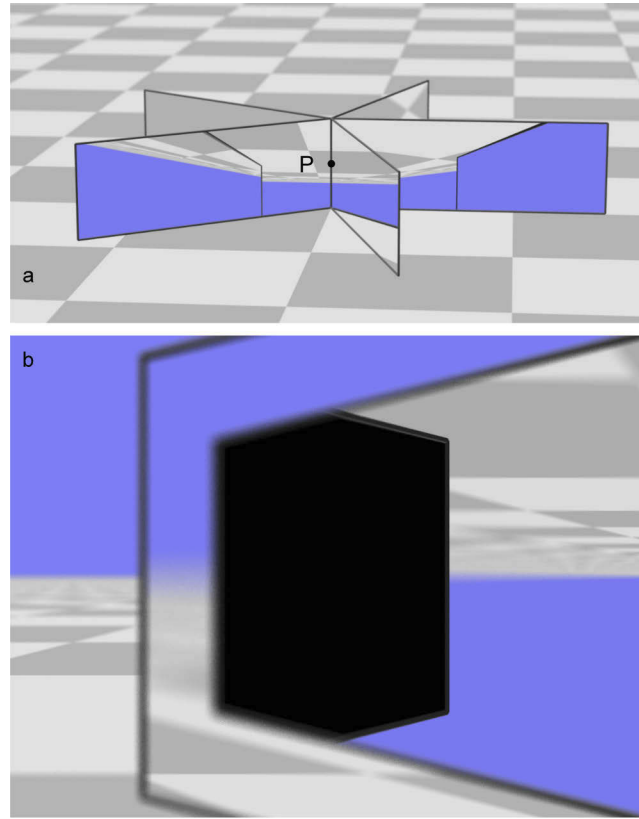
Fig. 1. Ray-tracing renderings of a lens star showing view from the outside (a) and from the inside (b). The location of the principal point P common to all lenses in the lens star, which always lies on the central straight line where all lenses intersect, is indicated in (a). The black areas visible in the centre of (b) correspond to rays that have not hit a light source after transmission through 100 lenses, which are rays in periodic orbits. See Appendix C. for information on the software used to create these images.
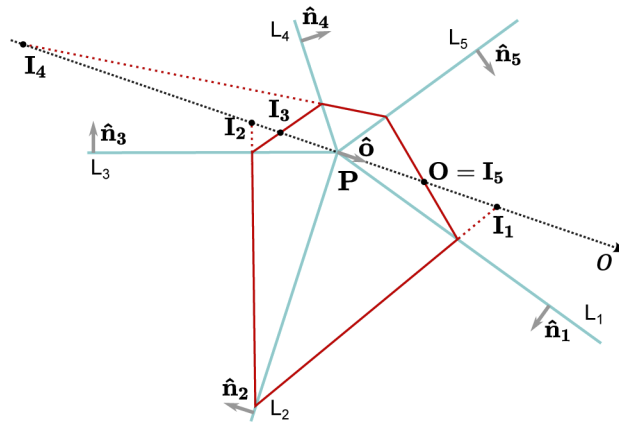

Fig. 2. Imaging due to a lens star.

in Ref. [18]) we can write

$$\mathbf{I}_k = \frac{\mathbf{I}_{k-1}}{1 + \mathbf{I}_{k-1} \cdot \hat{\mathbf{n}}_k / f_k} \, . \tag{2}$$

Here $\hat{\mathbf{n}}_k$ denotes the normal to the lens L_k and f_k its focal length; for the sake of generality, we are allowing the possibility when the lenses have different focal lengths. Multiplying both sides of Eq. (2) by vector $\hat{\mathbf{o}}$ and inverting then leads to the following expression

$$\frac{1}{\mathbf{I}_k \cdot \hat{\mathbf{o}}} = \frac{1}{\mathbf{I}_{k-1} \cdot \hat{\mathbf{o}}} + \frac{\hat{\mathbf{o}} \cdot \hat{\mathbf{n}}_k}{f_k} = \frac{1}{\mathbf{I}_{k-1} \cdot \hat{\mathbf{o}}} + \hat{\mathbf{o}} \cdot \mathbf{m}_k \, . \tag{3}$$

Here we have defined a vector $\mathbf{m}_k = \hat{\mathbf{n}}_k / f_k$ and used the fact that vectors $\mathbf{I}_{k-1}$ and $\hat{\mathbf{o}}$ are (anti)parallel and thus $\mathbf{I}_{k-1} \cdot \hat{\mathbf{n}}_k = (\mathbf{I}_{k-1} \cdot \hat{\mathbf{o}})(\hat{\mathbf{o}} \cdot \hat{\mathbf{n}}_k)$. Note that Eq. (3) is equivalent to Gaussian imaging equation ($-1/a + 1/b = 1/f_k$) for the special position of the point $\mathbf{I}_{k-1}$ on the axis of lens L_k when it holds that $\hat{\mathbf{o}} = \hat{\mathbf{n}}_k$, $a = \mathbf{I}_{k-1} \cdot \hat{\mathbf{o}}$ and $b = \mathbf{I}_k \cdot \hat{\mathbf{o}}$. To obtain the imaging equation due to n subsequent lenses, all we have to do is apply Eq. (3) repeatedly, each time with the respective normal $\hat{\mathbf{n}}_k$ of the kth lens L_k. Applying this procedure we finally obtain the imaging equation due to n subsequent lenses $L_1, \ldots, L_n$ of the lens star

$$\frac{1}{\mathbf{I}_n \cdot \hat{\mathbf{o}}} = \frac{1}{\mathbf{O} \cdot \hat{\mathbf{o}}} + \hat{\mathbf{o}} \cdot \sum_{k=1}^{n} \frac{\hat{\mathbf{n}}_k}{f_k} = \frac{1}{\mathbf{O} \cdot \hat{\mathbf{o}}} + \hat{\mathbf{o}} \cdot \mathbf{M} \, . \tag{4}$$

Here we have defined a vector $\mathbf{M} = \sum_{k=1}^{n} \mathbf{m}_k$; we can call $\mathbf{m}_k$ and $\mathbf{M}$ the "optical power vectors" of the lens L_k and of the whole system, respectively. Comparing Eqs. (3) and (4), we see that the combined imaging by the n lenses $L_1, \ldots, L_n$ is described formally by the same equation as imaging by a single lens L_k, just the optical power vector $\mathbf{m}_k$ is replaced by the vector $\mathbf{M}$. This way, any group of subsequent lenses within the lens star is equivalent to a single lens whose optical power vector is the sum of the optical power vectors of the individual lenses. This finding is closely related to the concept of the projected focal length developed in [23], namely the inverse of product $\hat{\mathbf{o}} \cdot \mathbf{M}$ corresponds to the projected focal length of the system to the o-axis.

With this result at hand, it is easy to find imaging by the regular lens star where all the lenses have the same focal length and are regularly angularly distributed. Due to such symmetry, $\mathbf{M} = \mathbf{0}$ holds and therefore the net imaging by the whole lens star is identity. This proves that the edge imaging condition is satisfied for the central axis of the lens star.

One of the consequences of this observation is that combined imaging by lenses $L_1, L_2, \ldots, L_k$ is the same as combined imaging by the remaining lenses $L_N, L_{N-1}, \ldots, L_{k+1}$ in the reverse order. This way, the view through the lens star is not "broken" by the star axis but it is smooth across it, as is shown in Fig. 3.
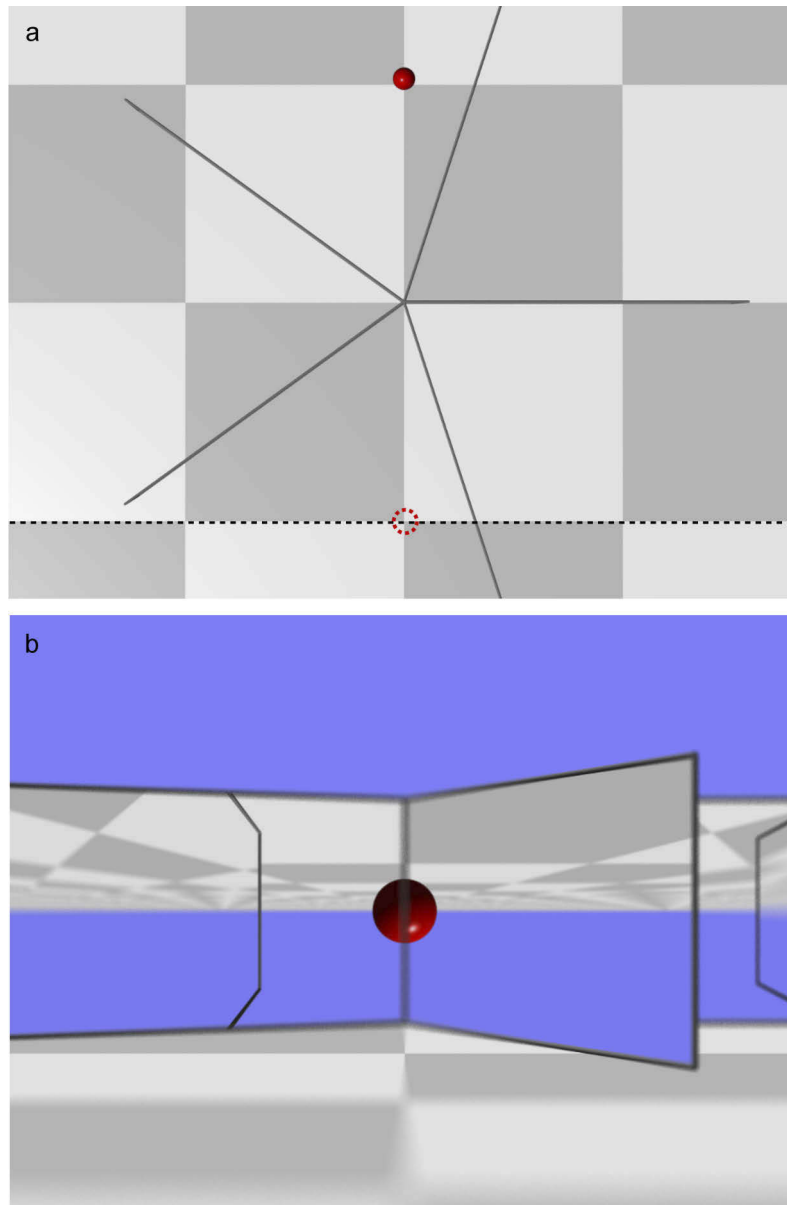
Fig. 3. Imaging to the opposite side. (a) Top view of a red sphere placed inside a lens star comprising $N = 5$ lenses, which produces an image of the sphere at the position indicated by the dotted red circle. (b) When viewed from a direction in which the red sphere is precisely behind the centre of the lens star, the image of the red sphere is seen in front of the centre of the lens star. The virtual camera, which has a very short depth of focus, is focused on a plane on which the image of the red sphere is centred (shown as a dotted black line in (a)); the image of the sphere is in focus, which shows that it is at the expected position. The image shown in (b) is simulated for a camera position located a distance 10 floor-tile lengths below the centre of the lens star in (a). See Appendix C. for information on the raytracing software.

3. Light-ray trajectories in a regular lens star

Let us consider a regular lens star, comprising N lenses of focal length f. We will denote $\delta = 2\pi/N$ the angle between two neighbouring lenses. For the sake of clarity, we will consider only those light rays propagating in a plane $\mathcal{P}$, which comprises the common principal point P and is perpendicular to the star axis; we will call this plane $\mathcal{P}$ the *canonical plane* of the lens star. Trajectories of light rays not lying in $\mathcal{P}$ are related to those lying in $\mathcal{P}$ via an orthogonal projection to the plane $\mathcal{P}$.

Let r_i denote the distance between the ray intersection with lens L_i and the principal point P. Further, let α_i denote the angle between the lens L_i and the ray emerging from it measured on the side more distant from P as depicted in Fig. 4. In Appendix A. we derive the following recursive formulas for the subsequent intersections:

$$r_i = \frac{r_{i-1}}{\cos \delta - \sin \delta \cot \alpha_{i-1}}, \tag{5}$$

$$\cot \alpha_i = \frac{1 + \cot \alpha_{i-1} \cot \delta - \frac{r_{i-1}}{f \sin \delta}}{\cot \delta - \cot \alpha_{i-1}}. \tag{6}$$

These formulas allow calculation of all the ray segments between the lenses from a given initial condition (initial ray). In the following we apply them to specific situations.
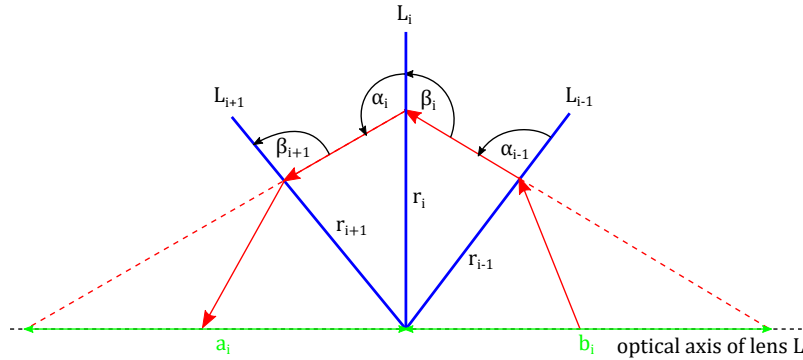

Fig. 4. The quantities characterising the ray propagating in a lens star.

3.1. Regular-polygon trajectory

A ray trajectory in a star lens may intersect all the lenses, or may not. In the former case, the ray trajectory forms a closed polygon due to the edge-imaging condition. A special case is ray trajectory in the form of a regular polygon for which all the distances r_i defined above are the same (and equal to the radius r of the circle escribed to the polygon), and also all the angles α_i are the same. If we in addition denote the radius of the circle inscribed in the polygon by R, there is a simple relation $R = r \cos(\delta/2)$ which, together with Eqs. (5) and (6) yields the following formula for the focal length f in terms of the regular trajectory radius R and the angle δ between neighbouring lenses:

$$R = 2f \sin \frac{\delta}{2} = 2f \sin \frac{\pi}{N}. \tag{7}$$

The radius R characterizes the lens star along with N and f and as we will see, in a sense is even more important than the latter ones. Therefore we will call R the *lens star parameter*.

3.2. Continuous lens star

It is interesting and instructive to consider the limit when both the number of lenses in the star N and the focal length f go to infinity, keeping the lens star parameter R given by Eq. (7) constant. We can call the resulting star as the *continuous lens star*. As we show in Appendix A.1, in this limit the light-ray trajectories become conic sections with one focus lying at the principal point P; they are described by the following equation in polar coordinates (r, φ):

$$r(\varphi) = \frac{R}{1 + e \cos(\varphi - \varphi_0)} . \tag{8}$$

As this equation shows, the parameter of all the conic sections in the continuous lens star is the same for all the rays and is equal to the parameter R of the lens star.

A few such ray trajectories are shown in Fig. 5. It is worth noting that these trajectories are the same as trajectories of a particle in Newton gravitational field (i.e., in the Kepler problem) with a fixed value of angular momentum [24]. On the other hand, it can be shown that there exists no radially symmetric refractive index profile that would give the same ray trajectories as the continuous lens star.
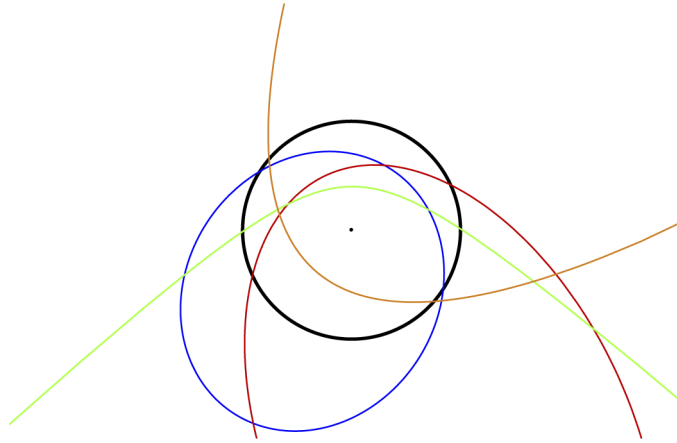

Fig. 5. Light rays in the continuous lens star are conic sections. The radius of the black circle, which the limiting case of the regular polygon ray trajectory, is equal to the lens star parameter R.

3.3. Ray properties in a finite lens star

There is an interesting feature of the light-ray trajectories in the lens stars with finite N illustrated in Fig. 6: a conic section can be inscribed to any such trajectory, and the points where the ray touches the conic section lies angularly half-way between the neighbouring lenses. It is not difficult to explain this behaviour using the results from Sec. 2. Indeed, imagine an alternative lens star with $N \to \infty$ lenses and the same parameter R as the lens star we are analysing. Now let us assume that lens L_1 of the original lens star lies along the x axis (more precisely, it lies in the plane xz, where the star axis coincides with the z axis). We will now prove that the wedge of angle δ placed symmetrically around the plane xz in the alternative lens star performs exactly the same imaging as the lens L_1 of the original lens star. To do that, we calculate the effective optical power vector $\mathbf{M}$ of that wedge as a sum of infinitesimal optical powers of infinitely many lenses contained in the wedge; it is not hard to see that it has just nonzero y component. Indeed, the infinitesimal optical power vectors have zero z components themselves so they do not contribute to M_z, and by symmetry of the wedge with respect to the plane xz, the x components of these

vectors mutually cancel, so $M_x = 0$ too. To find M_y, we have to perform transition to infinitely many lenses; if we denote by N the number of lenses in the full angle of 2π, then there will be $N\delta/(2\pi)$ lenses in the wedge spanning the angle δ. We also denote by f_c the focal length of these lenses. Then we get for the y component of **M**

$$M_y = \sum_{j=-N\delta/(4\pi)}^{N\delta/(4\pi)} \frac{1}{f_c} \cos \frac{2\pi j}{N} \rightarrow \frac{1}{f_c} \int_{-N\delta/(4\pi)}^{N\delta/(4\pi)} \cos \frac{2\pi j}{N}\, \mathrm{d}j = \frac{N}{2\pi f_c} \int_{-\delta/2}^{\delta/2} \cos \varphi\, \mathrm{d}\varphi = \frac{2\sin\frac{\delta}{2}}{R}. \quad (9)$$

In the last step we have taken advantage of Eq. (7) in the continuous star limit $N \rightarrow \infty$ that gives $R = 2\pi f_c/N$. Now, combining this result with Eq. (7) for the original lens star, we find $M_y = 1/f$. This way, the wedge of the continuous lens star defined above indeed images the same way as a single lens L_1 of the original lens star, and a similar consideration can be done for all the lenses L_k. Next, we can divide the original lens star into N wedge-shaped segments, each with angular span of δ placed symmetrically around one of the lenses. At the boundaries between these segments the rays in the original and in the alternative lens stars must coincide. Since we know that the rays in the alternative lens star form conic sections, the rays in the original lens star must be touching these conic sections at these points, which completes the proof.
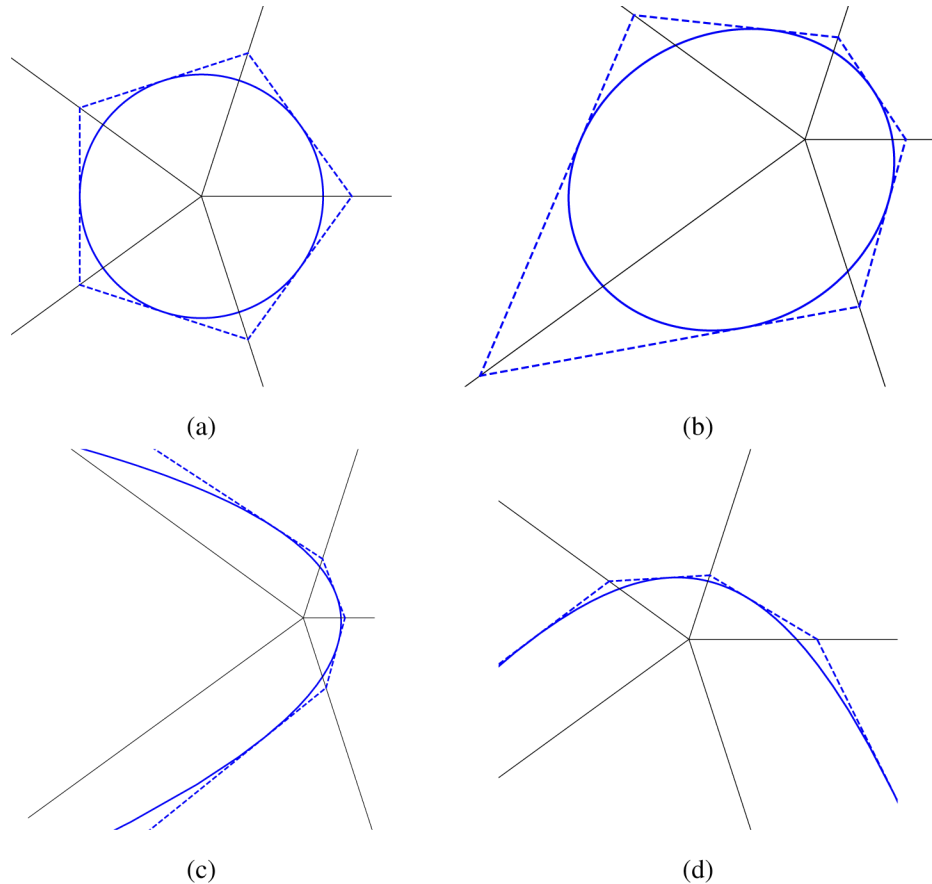

(a) (b)

(c) (d)

Fig. 6. Ray trajectories (dashed lines) in a star lens (here with $N = 5$) are tangential to the conic sections (full lines) that correspond to rays in the continuous star lens with the same parameter R. The corresponding conic sections are (a) circle, (b) ellipse, (c) parabola and (d) hyperbola.

We remind that these considerations are valid for rays lying in the canonical plane $\mathcal{P}$ of the lens star; other rays form conic sections as well, but they do not have their focus at the lens star principal point P any more.

3.4. Collimation by a half lens star

There is another interesting property of regular lens stars with the number of lenses N divisible by 4. Consider just half of such a star as depicted in Fig. 7 for N equal to 4, 20 and 100 (i.e., the numbers of lenses in the half-star are 2, 10 and 50, respectively). We can see that when rays are emitted from a point source S placed symmetrically on the axis of such a half-star at the distance R (the lens parameter), the rays get collimated. It is not difficult to explain this effect.
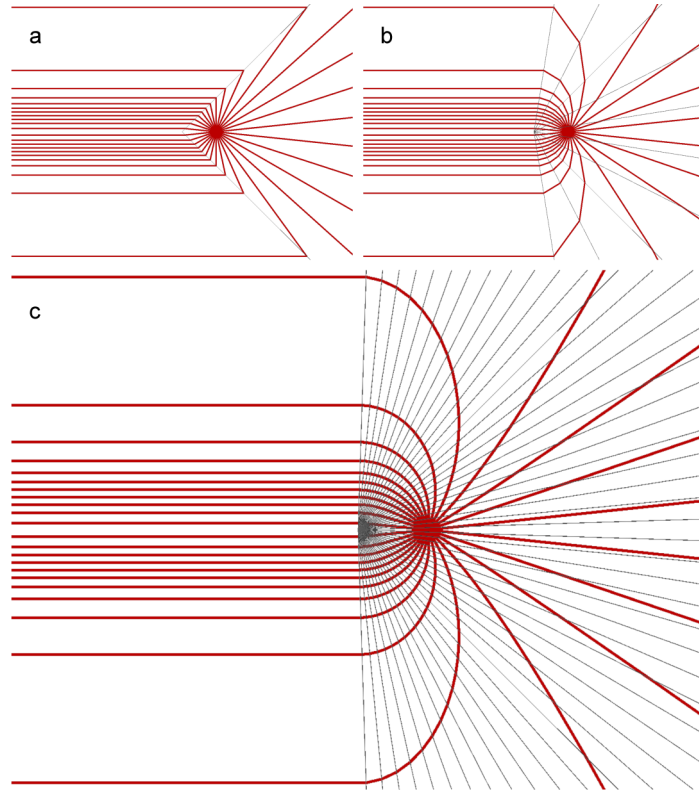

Fig. 7. Collimation by half a lens star. The number of lenses N in the full lens star is 4 (a), 20 (b), and 100 (c). The point light source is placed symmetrically at the distance R from the principal point on the axis of the half lens star. For details on the raytracing software used, see Appendix C.

Consider a ray emitted vertically upwards from the source S, (shown as ray 1 in Fig. 8). Since it starts at the distance R from the principal point P of the lenses, half-way between two lenses of the star, and perpendicularly to the straight line PS, it is exactly the ray forming the regular polygon. Therefore this ray, after being refracted by the $N/4$ lenses, will propagate horizontally because each of the lenses changes its direction by $2\pi/N$. Further, as we have shown above, the combined effect of a group of lenses in the star lens is the same as the effect of a single lens, whose optical power vector is the sum of optical power vectors of the individual lenses. This is true also for the $N/4$ lenses contained in the first quadrant ($x \geq 0, y \geq 0$). They can be replaced by a single effective lens that lies along the axis of the first quadrant. The orientation of the

lens follows from symmetry considerations and may be verified by calculating the optical power vector **M**. Now consider a ray emerging from the source S in the negative *x* direction (shown as ray 2 in Fig. 8). This ray passes through the principal point P of the effective lens, so it does not change its direction. This way, it becomes parallel with the first ray we considered earlier, i.e., the one starting from S vertically. We see that the effective lens redirects two different rays emerging from S to become parallel, which means that S lies in its focal plane. Therefore not only these two, but all rays emerging from S and passing through the $N/4$ lenses become parallel, which means that such a half lens star indeed collimates the rays as Fig. 7 shows. This argument remains valid also in the full 3D treatment: since the source S lies in the focal plane of the effective lens, all rays are redirected to form a collimated bundle, not just those lying in the canonical plane $\mathcal{P}$.
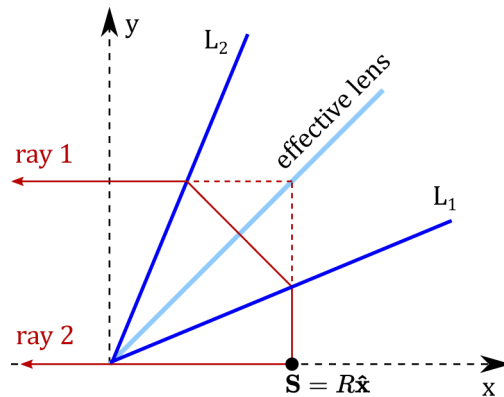

Fig. 8. The collimation by half lens star for $N = 8$. The $N/4 = 2$ lenses L_1 and L_2 can be replaced by the effective lens placed along the axis of the first quadrant. This lens makes two rays emerging from the point S parallel, which is then also true for other rays emerging from S.

4. Platonic lenses

In this section, we will present lens configurations inspired by Platonic solids and show the link between these structures and the lens stars already discussed.

Platonic solids are convex, regular polyhedra. There are 5 such polyhedra (Table 1). From each Platonic solid we will construct a corresponding *Platonic lens*, as follows: for each edge of the solid, a lens with focal length f is placed in a plane that contains that edge and the centre of the Platonic solid. The principal point of each lens coincides with the centre of the Platonic solid. Several examples of Platonic lenses are presented in Fig. 9.

Table 1. Table of the Platonic solids and a few of their properties.

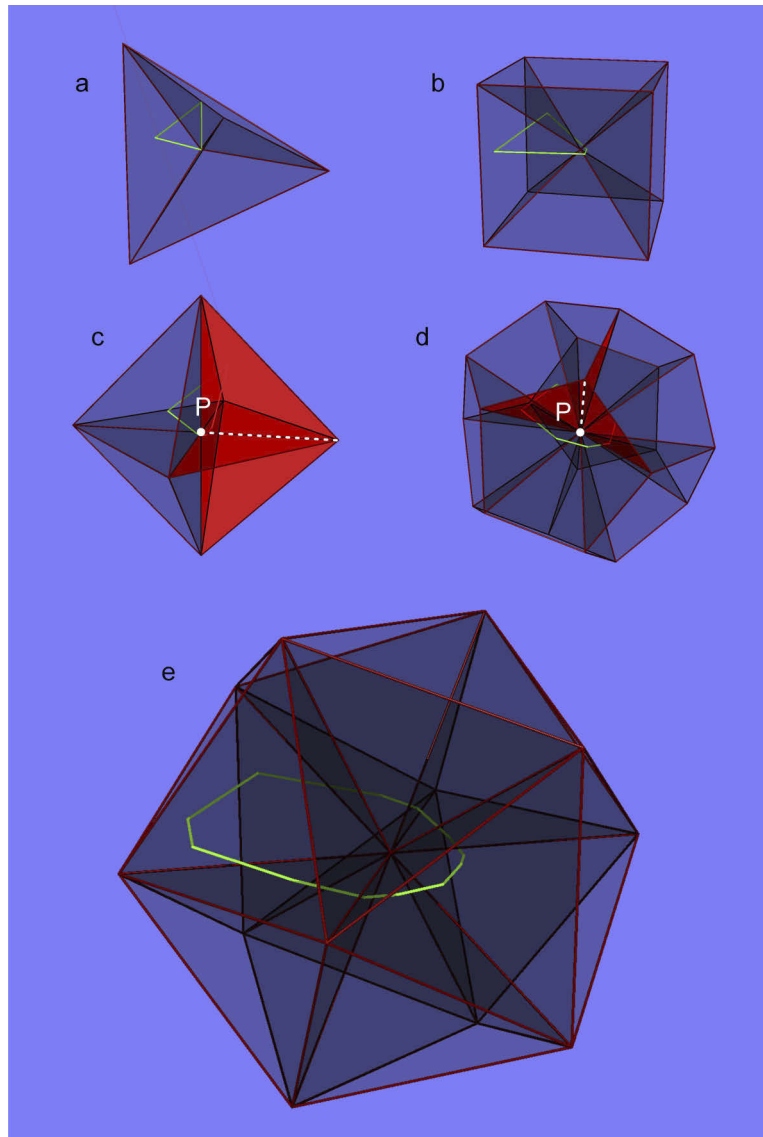| name	shape	faces	edges	vertices
tetrahedron		4	6	4
cube		6	12	8
octahedron		8	12	6
dodecahedron		12	30	20
icosahedron		20	30	12

Fig. 9. Closed trajectories (green lines) in different Platonic lenses, based on tetrahedron (a), cube (b), octahedron (c), dodecahedron (d), and icosahedron (e). In (c) and (d), the principal point, P, which is common to all lenses in a Platonic lens and which is located at the intersection point of all lenses, is indicated. Due to the symmetry, the lenses that intersect along any of the inner edges form a lens star. The planes of four lenses (shaded red) intersecting along a single line (dashed white line) and forming a lens star is highlighted in (c); similarly, three lenses forming a lens star are highlighted in (d). The focal length of each lens was chosen to equal the length of the inner edges. The trajectory shown inside the Platonic lens based on the cube can be understood as passing through all four vertical lenses, which (if extended to the vertical line through the centre of the cube) form a regular star of four lenses. To clarify the structure of the Platonic lenses, each lens was slightly shaded. Appendix C. contains information about the raytracing software.

Now we will show that the edge-imaging condition is satisfied for the inner edges of a Platonic lens built in this way: Consider one of the vertices of the Platonic solid, and consider all lenses

that intersect in the line from the centre of the solid to the chosen vertex. Because of the high symmetry of the Platonic solid, those lenses form a regular lens star and thus the edge-imaging condition is satisfied for their intersection line. Since the whole Platonic lens is a collection of these regular lens stars — one centred on each inner edge —, the edge-imaging condition is automatically satisfied for all inner edges of the Platonic lens. This, in turn, implies that the loop-imaging condition is satisfied for every closed loop inside a Platonic lens. Note that such a closed loop may not enclose any of the outer edges of the Platonic lens, which can be avoided by considering Platonic lenses with infinite radius. The inside of a Platonic lens therefore satisfies the loop-imaging condition, so the combination of all the lenses encountered along any closed loop inside a Platonic lens images any object point to itself.

Figure 9 supports the statement that the loop-imaging condition is satisfied inside different Platonic lenses: the presented light-ray trajectories form closed loops and thus any point lying on such light-ray is imaged back to itself due to the Platonic lens. As the centre of the Platonic lens is the principal point of each constituent lens, there is again an image line, i.e. the image of any point light source lies on a straight line through the point light source and the centre. As any point on a light-ray trajectory is such a point light source, the neighbouring segments of the trajectory pass through a point on the straight line through the point light source and the centre of the Platonic lens. Considering two points on one segment of a light-ray trajectory in this way then implies that the neighbouring segments of the trajectory lie in the plane containing the initial light-ray-trajectory segment and the centre of the Platonic lens, which in turn means that the *entire* trajectory lies in this plane. (In fact, this is more generally the case in any structure of glenses that satisfy the edge-imaging condition for all edges in the structure and that share a common nodal point.)

A ray trajectory in a Platonic lens may be quite complicated. There is in general no single conic section to which all ray segments would be tangent because there are in general several lens stars involved in the trajectory of a single ray. However, the fact that the whole ray lies in a single plane is very interesting and important.
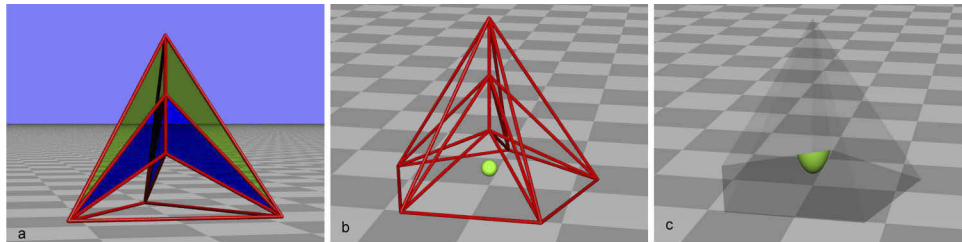

Fig. 10. Raytracing simulations of an original omnidirectional lens/ideal-lens cloak constructed around three-lens stars [18,19] (a) and its generalisation constructed around five-lens stars (b,c). The structure of these devices is shown in (b) and (c), where each planar polygon formed by red rods indicates the outline of a lens. In (a), the positions of lenses that form part of lens stars are shown shaded in green (upper lens star) and blue (lower lens star). In (b), a green sphere has been placed inside the rod model. In (c), which shows the appearance of the device with the rods removed and the lenses inserted, it can be seen that the green sphere appears distorted and is only partially visible, unlike any object (here the checkerboard floor) seen through the device, which appears undistorted. The lenses have been made slightly absorbing (specifically, the transmission coefficient of each lens was set to 0.96) so that the outline of the device can be seen. See Appendix C. for information about the raytracing software.

5. Generalised omnidirectional lens

The omnidirectional lens/ideal-lens cloak described in Refs. [18,19] contains two lens stars, each comprising three lenses (see Fig. 10(a)). This observation suggests that analogous lens structures that are constructed around lens stars with a greater number of lenses might also form TO devices. That this is indeed the case for lens stars comprising 5 lenses can be seen in the remaining panels of Fig. 10: Fig. 10(b) shows the structure of the device and the size and location of an object placed inside the structure; Fig. 10(c) shows that the appearance of the device is that expected of a TO device: any object seen through the device appears undistorted, but interior objects appear distorted according to the "transformation" between physical and virtual space.

6. When designing TO devices from ideal lenses, can unsuitable ideal-lens structures be eliminated by considering only principal-point conditions?

When designing our ideal-lens cloak [18], we proceeded as follows. First, we considered only the simple conditions on the principal-point positions that follow from the loop-imaging condition [20], and by a process of trial and elimination identified an ideal-lens structure that satisfied these conditions. Then we calculated the focal lengths of all the lenses in this structure such that all lenses with common edges satisfy the edge-imaging condition. The first step was quick and easy, the second slow and laborious.

Even if a lens structure satisfied all principal-point conditions, it is not at all obvious that there would be a combination of allowed (real-valued and non-zero) focal lengths that satisfies the edge-imaging condition for all edges simultaneously. We were therefore slightly surprised to find just such a focal-length combination for the very first ideal-lens structure for which we tried to find it, which poses the following question: *if a combination of ideal thin lenses satisfies the conditions on the principal-point positions due to the edge-imaging condition, does this imply that it is possible to find focal lengths for these lenses such that they form a TO structure?* If the answer was "Yes", then this would greatly facilitate the elimination of *all* unsuitable ideal-lens structures.

Unfortunately, the answer to the question is "No". We arrive at this conclusion by constructing an ideal-lens structure based on a lens star or Platonic lens that satisfies the principal-point conditions, but for which there is no choice of *non-zero* focal lengths that satisfies the edge-imaging condition for all edges in the structure. The details of the construction and calculation are technical and laborious; they can be found in Appendix B.

This result leaves a number of related questions unanswered.

1. If an ideal-lens structure satisfies the principal-point conditions, are there always consistent, real-valued, solutions for the focal lengths if we allow focal length 0?

2. Are there additional conditions on the principal points which, when satisfied, guarantee that allowed and consistent solutions for the focal lengths exist?

7. Physical realisability of lens stars

In our calculations, we have considered ideal thin lenses so far. Therefore, a natural question arises: how do our results change if real lenses are implemented?

Lenses are commonly used and well understood optical elements, but designing and manufacturing novel types of lenses is a highly active field of research and yields impressive outcomes. The reason for this research is the limited functionality of conventional lenses, which are optimised for imaging objects lying on the optical axis. Images of off-axis objects suffer from several aberrations, e.g. barrel distortion (when straight lines are imaged to curved lines in the shape of a barrel) or coma (when an off-axis point appears to have a tail), chromatic aberration, etc. All

these aberrations degrade the image quality beyond the paraxial regime, in which the light rays form small angles with the optical axis.

Figure 11 shows the effect of replacing ideal lenses with holographic lenses on two light-ray trajectories. Figure 11(a) shows two light-ray trajectories in an ideal-lens star. Both trajectories are piecewise tangential to conic sections, here a parabola and an ellipse. Figure 11(b) shows two light-ray trajectories starting from the same positions and in the same directions in the same lens star, but with each ideal lens replaced by a phase hologram that introduces a phase shift which varies quadratically with distance from the principal point, a type of holographic lens that works well paraxially. Both trajectories are drastically different, ultimately because the holographic lenses are used non-paraxially, and the precession evident (in one case upon close inspection) in both trajectories shows that none are piecewise tangential to conic sections any longer. Other lens-hologram designs are possible, and Fig. 11(c) shows two trajectories in a holographic lens star optimised for all light rays that pass through one particular point, P. Those light rays are then deflected precisely as they would by an ideal-lens star. The point P was chosen to be the starting point of one of the trajectories, and – as expected – that trajectory can be seen to be precisely the same as the corresponding trajectory in the ideal-lens star. The other trajectory, which does not pass through the point P, is very different from its ideal-lens-star counterpart. Note that the half-lens stars shown in Fig. 7 can be made holographic and optimised by for the point-light-source position. We have performed the corresponding simulations, but are not showing them here as they look identical to those shown in Fig. 7, as they should. Holographic lens stars optimised in this way might be employed in applications when the light source is fixed near a particular position, e.g. in diffraction experiments or in microscope illumination systems.
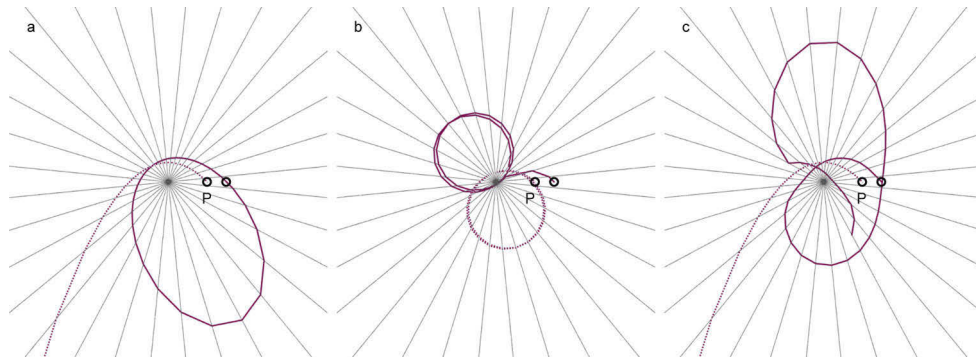

Fig. 11. Two ray trajectories (one dotted, one solid) in an ideal-lens star (a), in a lens star comprising holographic lenses with a quadratic phase profile (b), and in a holographic lens star optimised for rays passing through the point P, which is also the starting position of the dotted trajectory (c). The two trajectories start at different positions, marked by black circles. In (a), both trajectories follow conic sections (more precisely: they are piecewise tangential to a conic section), a parabola (dotted trajectory) and an ellipse (solid trajectory). In (b), both trajectories are completely different from those in (a). In (c), the dotted trajectory is identical to the dotted trajectory in (a), but the solid trajectory is different. Note that the holographic lenses occasionally reflect rays, namely when the phase gradient added by the hologram would make the ray's phase gradient greater than $2\pi/\lambda$. For details on the raytracing software used, see Appendix C.

Another promising experimental realisation of lens stars and Platonic lenses would employ metalenses [25–29], that is lenses realised using thin metasurfaces, which are taking great strides in the direction of ideal thin lenses [30]. Metalenses have many degrees of freedom that can be altered to address the shortcomings of planar phase holograms with a quadratic phase profile. For example, they can be non-planar and phase profiles non-parabolic to reduce coma and spherical

aberration [31], and the complexities of the metasurface can be used to address shortcomings such as dispersion [32,33]. The rapid progress in developing and fabricating metalenses makes researchers to believe that even closer approximations of ideal thin lenses with reduced aberrations such as coma will be built in the near future [34].

8. Conclusions

We have investigated lens stars composed of equiangularly spaced lenses of the same power and described imaging by such a star and a part of it. Introducing the concept of continuous lens star as the limit when the number of lenses goes to infinity, we have shown that light rays in such stars form conic sections with their focus at the star centre. Establishing equivalence of a segment of a finite lens star with a segment of a continuous lens star, we have further shown that rays in lens stars are tangent to conic sections. We have introduced Platonic lenses as lens systems based on Platonic solids and shown that the edge-imaging condition is satisfied by the lens stars contained in it. We have also discussed some possible applications of the proposed devices, namely the ray collimator based on a half lens star and the relation of lens stars to transformation optics devices which may pave the way to invisibility cloaks based on lens star systems. It is possible to extend these ideas in different directions; for example, one may think of lens stars with unequally spaced lenses of unequal power, investigate ray trajectories in complex TO structures based on Platonic lenses etc. We leave these questions for further research.

Appendix A. Calculation of the light-ray trajectories

We denote the distances and angles as is shown in Fig. 4. Then we have the following relations:

$$\frac{a_i}{r_i} = \cot\left(\alpha_i - \frac{\pi}{2}\right) = -\tan\alpha_i \tag{10}$$

$$\frac{b_i}{r_i} = \cot\left(\beta_i - \frac{\pi}{2}\right) = -\tan\beta_i \tag{11}$$

The lens equation then gives

$$\frac{1}{a_i} + \frac{1}{b_i} = \frac{1}{f} \tag{12}$$

From Fig. 4 we also see the following relations for the angles between the ray and lenses L_{i-1} and L_i:

$$\beta_i = \pi + \delta - \alpha_{i-1} \tag{13}$$

and from the sine theorem we get

$$r_{i-1} \sin\alpha_{i-1} = r_i \sin\beta_i = r_i \sin(\alpha_{i-1} - \delta). \tag{14}$$

Putting Eqs. (10), (11), (12), (13) and (14) together, we get a recursive formulas that enable to calculate r_i and $\cot\alpha_i$ from r_{i-1} and $\cot\alpha_{i-1}$:

$$r_i = r_{i-1} \frac{\sin\alpha_{i-1}}{\sin(\alpha_{i-1} - \delta)} = \frac{r_{i-1}}{\cos\delta - \sin\delta \cot\alpha_{i-1}}, \tag{15}$$

$$\cot\alpha_i = \cot(\alpha_{i-1} - \delta) - \frac{1}{f} \frac{r_{i-1}}{\cos\delta - \sin\delta \cot\alpha_{i-1}} = \frac{1 + \cot\alpha_{i-1}\cot\delta - \frac{r_{i-1}}{f\sin\delta}}{\cot\delta - \cot\alpha_{i-1}}. \tag{16}$$

These relations enable us to calculate the positions of intersection of the ray with the respective lenses.

A.1. The limit $N \to \infty$

Consider the case when the number of lenses goes to infinity with the lens parameter R kept constant. We would like to derive some form of differential equations for the trajectory from relations (15) and (16). To do that, we take advantage of the fact that in the limit $N \to \infty$ the angle δ goes to zero, and we can express the contangens and sine of the angle $(\alpha_{i-1} - \delta)$ in Eqs. (15) and (16) by the Taylor expansion to the first order as follows,

$$\sin(\alpha_{i-1} - \delta) = \sin \alpha_{i-1} - \delta \cos \alpha_{i-1} \tag{17}$$

$$\cot(\alpha_{i-1} - \delta) = \cot \alpha_{i-1} + \frac{\delta}{\sin^2 \alpha_{i-1}} \tag{18}$$

We also define the increments of α and d between successive lenses as $\Delta\alpha_i \equiv \alpha_i - \alpha_{i-1}$ and $\Delta r_i \equiv r_i - r_{i-1}$. Taking again into account that these increments are small and using again Taylor expansion up to the first order, we can rewrite Eqs. (15) and (16) as

$$\Delta\alpha_i = -\delta + \frac{r_{i-1}}{f} \sin^2 \alpha_{i-1}(1 + \delta \cot \alpha_{i-1}) \tag{19}$$

$$\Delta r_i = \delta \, r_{i-1} \cot \alpha_{i-1} \tag{20}$$

Now as the number of lenses N increases, their focal length also increases to keep the lens parameter $R = 2f \sin(\delta/2)$ constant, so for large N we can set $f = R/\delta$. Inserting this into Eqs. (19) and (20), keeping only terms up to the first order in δ, we obtain

$$\frac{\Delta\alpha_i}{\delta} = \frac{r_{i-1}}{R} \sin^2 \alpha_{i-1} - 1 \tag{21}$$

$$\frac{\Delta r_i}{\delta} = r_{i-1} \cot \alpha_{i-1} \tag{22}$$

Now, in the limit $\delta \to 0$ the ratios $\Delta\alpha_i/\delta$ and $\Delta r_i/\delta$ simply go to the derivatives of α and r with respect to the polar angle φ because δ is just the change of the polar angle when going from one lens to the next. We can therefore replace these expressions by the derivatives, omitting the index $i-1$ as we go from difference equations to differential ones. This way, we get a system of two equations

$$\alpha' = \frac{r}{R} \sin^2 \alpha - 1 \tag{23}$$

$$r' = r \cot \alpha, \tag{24}$$

where the prime denotes the derivative with respect to φ.

One can eliminate α from this system of equation by differentiating the second one and making suitable substitutions. The result is the equation

$$r'' = \frac{2r'^2}{r} + r - \frac{r^2}{R} \, . \tag{25}$$

To solve this equation, we make a substitution $r = 1/\xi$, which yields the equation for ξ

$$\xi'' + \xi - \frac{1}{R} = 0 \tag{26}$$

with the simple solution that can be written as $\xi(\varphi) = [1 + e \cos(\varphi - \varphi_0)]/R$, which then yields

$$r(\varphi) = \frac{R}{1 + e \cos(\varphi - \varphi_0)} \, . \tag{27}$$

This shows that the ray trajectories in the continuous lens star have the shape of conic sections, all with the same parameter R. The values of parameters e and φ_0 can be calculated from the

initial conditions $r(0) = r_0$ and $\frac{\mathrm{d}r}{r\mathrm{d}\varphi}|_{\varphi=0} = D$ as

$$\cos\varphi_0 = \frac{\frac{R}{r_0} - 1}{e}, \tag{28}$$

$$e = \sqrt{\left(\frac{DR}{r_0}\right)^2 + \left(\frac{R}{r_0} - 1\right)^2}. \tag{29}$$

Appendix B. Investigating the edges and calculating the focal lengths of lenses in a star cloak

Consider a star cloak, depicted in Fig. 12(a). In Ref. [20], we have derived the conditions on the relative principal-point positions of lenses intersecting in a common edge to satisfy the edge-imaging condition, provided that the focal lengths of the intersecting lenses are chosen such that the combination provides the identity mapping. Let us recall two of those rules, which will be applied on the edges in the star cloak: the principal points of three intersecting lenses must coincide and the principal points of four intersecting lenses must lie on a straight line.
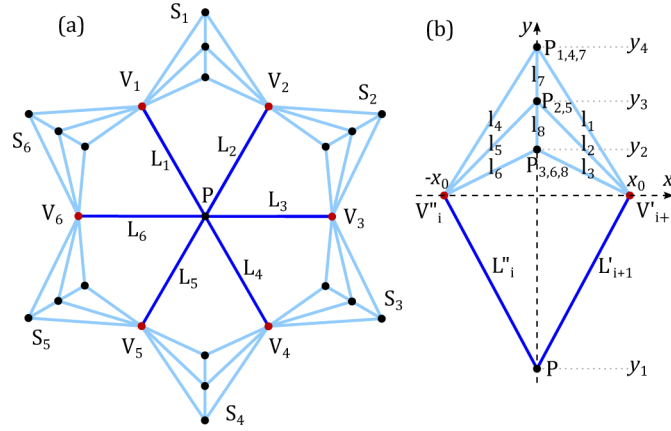

Fig. 12. The "star cloak". Lens L_i with a focal length f from the regular lens star is considered as a pair of coinciding lenses L'_i and L''_i, each with a focal length $2f$. Edge V_i can be regarded as a pair of coinciding edges, V'_i and V''_i. At the edge V'_i, lenses l_4, l_5, l_6 and L'_i intersect, whereas V'_i represents the intersection of lenses l_1, l_2, l_3 and L''_i. $P_{i,j,...}$ represents the common principal point of lenses l_i, l_j,....

From Fig. 12(b), one can deduce that these rules are satisfied for those edges of structures S_i (cyan lines) containing cumulated principal points $P_{3,6,8}$, $P_{2,5}$ and $P_{1,4,7}$ ($P_{i,j, ...}$ represents the common principal point of lenses l_i, $l_j, ...$ sincluded in the structure S). What remains is to show that the edge-imaging condition holds also for the edges V_i, where even seven lenses intersect. For this goal, we will use the fact that lens L_i of focal length f can be regarded as a pair of coinciding lenses L'_i and L''_i, each with a focal length $2f$. Then, edge V_i can be also considered as a pair of coinciding edges V'_i and V''_i, each corresponding to the intersection of four lenses (see Fig. 12(b)). Now, the principal points of the foursome of lenses intersecting at that edge lie on a straight line; the same holds for the edge V''_i. Since the principal-point condition is satisfied for edges V'_i and V''_i individually, it is also satisfied for the original edge V_i. Therefore, in principal, the edge-imaging condition can be satisfied for all the edges in a star cloak.

We checked it by calculating the focal lengths $f_1, \ldots, f_8$ of lenses $l_1, \ldots, l_8$; the common focal length f of the lenses L_i from the lens star was treated as a free parameter. Employing

the formulas derived in Ref. [18], we found out that there is only one way how to calculate the focal lengths $f_1, \ldots, f_6$. However, the remaining focal lengths f_7 and f_8 can be calculated in two different ways, because both lenses l_7 and l_8 show in two different lens intersections: one edge of lens l_7 can be found in an intersection of lenses l_1, l_4 and l_7, whereas the other edge of l_7 shows in an intersection of four lenses l_2, l_5, l_8 and l_7. Similarly, one edge of lens l_8 occurs in an intersection of lenses l_3, l_6 and l_8, whereas the other edge of l_8 can be found in an intersection of four lenses l_2, l_5, l_7 and l_8.

First, we calculated focal lengths $f_1, \ldots, f_6$ using Eqns (25) from Ref. [18] (which refers to asymmetric four-lens intersection), substituting $f_{11} \rightarrow 2f$, $f_{10} \rightarrow f_3$, $f_9 \rightarrow f_2$, $f_8 \rightarrow f_1$ (by symmetry, $f_4 = f_1$, $f_5 = f_2$, $f_6 = f_3$), $y_{11} \rightarrow y_1$, $y_{10} \rightarrow y_2$, $y_9 \rightarrow y_3$ and $y_8 \rightarrow y_4$. Then, we calculated f_7 using Eq. (8) from the same reference (which refers to a symmetric three-lens intersection), substituting $f_1 \rightarrow f_1$, $f_2 \rightarrow f_7$ and $\cos \alpha \rightarrow y_4 / \sqrt{x_0^2 + y_4^2}$. After that, we calculated f_8 using Eq. (9) from [18] (which refers to a mirror-symmetric four-lens intersection), substituting $f_5 \rightarrow f_8$, $f_7 \rightarrow f_7$, $h_5 \rightarrow y_4 - y_3$ and $h_7 \rightarrow y_2 - y_3$. Finally, we compared the obtained value of f_8 with a value f_8' of the focal length of lens l_8, obtained by employing Eq. (8) from [18], substituting $f_1 \rightarrow f_3$, $f_2 \rightarrow f_8$ and $\cos \alpha \rightarrow -y_2 / \sqrt{x_0^2 + y_2^2}$. The calculation, presented in [35], showed that the difference $f_8 - f_8'$ is generally non-zero. To make $f_8 - f_8' = 0$, one can choose either $y_1 = 0$ or $x_0(y_1 - y_2)(y_1 - y_4) + 2f \sqrt{x_0^2 + y_1^2}(y_2 - y_4) = 0$. The condition $y_1 = 0$ corresponds to the trivial case of two mirror-symmetric omnidirectional lenses, whose base lenses coincide. The other condition being satisfied leads to the unphysical case when $f_3 = f_6 = f_1 = f_4 = f_7 = f_8 = 0$. This calculation for $y_1 \neq 0$ shows that even when the principal-point conditions are satisfied for each edge of the ideal-lens device, it is not guaranteed that it is possible to choose (non-zero) focal lengths of the considered lenses such that the edge-imaging condition is satisfied everywhere in the device. We have also performed an analogous calculation for a three-dimensional device (which could be called a *platonic cloak*), leading to the same result, i.e. for the device to be a TO device, either $y_1 = 0$ or focal lengths of some lenses must be zero. This calculation is also presented in [35].

Appendix C. Raytracing simulations

All raytracing simulations shown in this paper were performed using our open-source raytracer Dr TIM [36,37]. Dr TIM traces rays backwards, starting from the camera and ending in a light source. Compared to tracing light rays forwards, starting from a light source, this is very efficient as only light rays that enter the camera — a tiny fraction of all light rays — are being traced. However, many aspects of illumination are not simulated correctly.

Since the publication of Ref. [36], Dr TIM's code has been significantly extended. Extensions relevant to this paper can be found in two packages:

- `LensStar` (`optics.raytrace.research.LensStar`), which contains classes related to the visualisation of lens stars, and

- `PlatonicLens` (`optics.raytrace.research.PlatonicLens`), which is a collection of classes that visualise Platonic lenses.

Further relevant classes are linked from the classes in these packages.

The images shown in Figs. 1 and 3 were created using the `LensStarRenderer` class in the `LensStar` package.

Figure 5 was created with the software Mathematica.

Figure 6 was created using the `LensStarConicSectionTrajectoryPlotter` class in the `LensStar` package.

The simulations shown in Fig. 7 was performed using the `LensStarPointLightSourceTrajectoryPlotter` class in the `LensStar` package.

Figure 9 was calculated using the `PlatonicLensTrajectoryPlotter` class (`PlatonicLens` package).

Figure 11 used the `HolographicLensStarConicSectionTrajectoryPlotter` class (`LensStar` package).

Finally, Fig. 10 was created with the interactive `TIMJavaApplication` class in the `optics.raytrace` package. The scene was initialised to the *Minimalist* scene, which consists of a checkerboard floor and a blue sky. A new `Ideal-lens cloak` was added to the scene, with the `No of base vertices` parameter set to 3 in (a) and 5 in (b) and (c). For (a), the ideal-lens cloak was then converted into a collection of scene objects, and the `Visible` and `Surface` parameter of individual scene objects in this collection adjusted.

Disclosures. The authors declare no conflicts of interest.

Data availability. No data were generated or analyzed in the presented research.

References

1. J. B. Pendry, D. Schurig, and D. R. Smith, "Controlling Electromagnetic Fields," Science **312**(5781), 1780–1782 (2006).
2. U. Leonhardt and T. G. Philbin, "General Relativity in Electrical Engineering," New J. Phys. **8**(10), 247 (2006).
3. D. A. Genov, S. Zhang, and X. Zhang, "Mimicking celestial mechanics in metamaterials," Nat. Phys. **5**(9), 687–692 (2009).
4. H. Chen, S. Tao, J. Bělín, J. Courtial, and R.-X. Miao, "Transformation cosmology," Phys. Rev. A **102**(2), 023528 (2020).
5. R. Schittny, M. Kadic, S. Guenneau, and M. Wegener, "Experiments on transformation thermodynamics: molding the flow of heat," Phys. Rev. Lett. **110**(19), 195901 (2013).
6. R. Hu, X. Wei, J. Hu, and X. Luo, "Local heating realization by reverse thermal cloak," Sci. Rep. **4**(1), 3600 (2015).
7. B.-I. Popa, L. Zigoneanu, and S. A. Cummer, "Experimental acoustic ground cloak in air," Phys. Rev. Lett. **106**(25), 253901 (2011).
8. N. Stenger, M. Wilhelm, and M. Wegener, "Experiments on elastic cloaking in thin plates," Phys. Rev. Lett. **108**(1), 014301 (2012).
9. S. Brûlé, E. Javelaud, S. Enoch, and S. Guenneau, "Experiments on seismic metamaterials: Molding surface waves," Phys. Rev. Lett. **112**(13), 133901 (2014).
10. F. Monticone and A. Alù, "Invisibility exposed: physical bounds on passive cloaking," Optica **3**(7), 718–724 (2016).
11. X. Chen, Y. Luo, J. Zhang, K. Jiang, J. B. Pendry, and S. Zhang, "Macroscopic invisibility cloaking of visible light," Nat. Commun. **2**(1), 176 (2011).
12. B. Zhang, Y. Luo, X. Liu, and G. Barbastathis, "Macroscopic invisibility cloak for visible light," Phys. Rev. Lett. **106**(3), 033901 (2011).
13. H. Chen and B. Zheng, "Broadband polygonal invisibility cloak for visible light," Sci. Rep. **2**(1), 255 (2012).
14. H. Chen, B. Zheng, L. Shen, H. Wang, X. Zhang, N. Zheludev, and B. Zhang, "Ray-optics cloaking devices for large objects in incoherent natural light," Nat. Commun. **4**(1), 2652 (2013).
15. J. S. Choi and J. C. Howell, "Paraxial ray optics cloaking," Opt. Express **22**(24), 29465–29478 (2014).
16. S. Oxburgh, C. D. White, G. Antoniou, E. Orife, T. Sharpe, and J. Courtial, "Large-scale, white-light, transformation optics using integral imaging," J. Opt. **18**(4), 044009 (2016).
17. T. Tyc, S. Oxburgh, E. N. Cowie, G. J. Chaplain, G. Macauley, C. D. White, and J. Courtial, "Omnidirectional transformation-optics cloak made from lenses and glenses," J. Opt. Soc. Am. A **33**(6), 1032–1040 (2016).
18. J. Courtial, T. Tyc, J. Bělín, S. Oxburgh, G. Ferenczi, E. N. Cowie, and C. D. White, "Ray-optical transformation optics with ideal thin lenses makes omnidirectional lenses," Opt. Express **26**(14), 17872–17888 (2018).
19. J. Bělín, T. Tyc, M. Grunwald, S. Oxburgh, E. N. Cowie, C. D. White, and J. Courtial, "Ideal-lens cloaks and new cloaking strategies," Opt. Express **27**(26), 37327–37336 (2019).
20. T. Tyc, J. Bělín, S. Oxburgh, C. D. White, E. N. Cowie, and J. Courtial, "Combinations of generalized lenses that satisfy the edge-imaging condition of transformation optics," J. Opt. Soc. Am. A **37**(2), 305–315 (2020).
21. J. E. Greivenkamp, *Field guide to geometrical optics*, vol. 1 (SPIE press Bellingham, WA, 2004).
22. A. Gerrard and J. M. Burch, *Introduction to matrix methods in optics* (Courier Corporation, 1994).
23. J. Bělín and J. Courtial, "Imaging with two skew ideal lenses," J. Opt. Soc. Am. A **36**(1), 132–141 (2019).
24. L. D. Landau and E. M. Lifshitz, *Mechanics: Volume 1*, vol. 1 (Butterworth-Heinemann, 1976).
25. N. Yu, P. Genevet, M. A. Kats, F. Aieta, J.-P. Tetienne, F. Capasso, and Z. Gaburro, "Light propagation with phase discontinuities: generalized laws of reflection and refraction," Science **334**(6054), 333–337 (2011).

26. X. Ni, A. V. Kildishev, and V. M. Shalaev, "Metasurface holograms for visible light," Nat. Commun. **4**(1), 2807 (2013).

27. G. Zheng, H. Mühlenbernd, M. Kenney, G. Li, T. Zentgraf, and S. Zhang, "Metasurface holograms reaching 80% efficiency," Nat. Nanotechnol. **10**(4), 308–312 (2015).

28. L. Wang, S. Kruk, H. Tang, T. Li, I. Kravchenko, D. N. Neshev, and Y. S. Kivshar, "Grayscale transparent metasurface holograms," Optica **3**(12), 1504–1505 (2016).

29. P. Genevet, F. Capasso, F. Aieta, M. Khorasaninejad, and R. Devlin, "Recent advances in planar optics: from plasmonic to dielectric metasurfaces," Optica **4**(1), 139–152 (2017).

30. H. Liang, A. Martins, B.-H. V. Borges, J. Zhou, E. R. Martins, J. Li, and T. F. Krauss, "High performance metalenses: numerical aperture, aberrations, chromaticity, and trade-offs," Optica **6**(12), 1461–1470 (2019).

31. F. Aieta, P. Genevet, M. Kats, and F. Capasso, "Aberrations of flat lenses and aplanatic metasurfaces," Opt. Express **21**(25), 31530–31539 (2013).

32. S. Shrestha, A. C. Overvig, M. Lu, A. Stein, and N. Yu, "Broadband achromatic dielectric metalenses," Light: Sci. Appl. **7**(1), 85 (2018).

33. W. T. Chen, A. Y. Zhu, V. Sanjeev, M. Khorasaninejad, Z. Shi, E. Lee, and F. Capasso, "A broadband achromatic metalens for focusing and imaging in the visible," Nat. Nanotechnol. **13**(3), 220–226 (2018).

34. H.-T. Chen, A. J. Taylor, and N. Yu, "A review of metasurfaces: physics and applications," Rep. Prog. Phys. **79**(7), 076401 (2016).

35. J. Bělín, T. Tyc, and J. Courtial, "Mathematica notebooks related to lens stars and platonic lenses," http://dx.doi.org/10.6084/m9.figshare.15062688 (2021).

36. S. Oxburgh, T. Tyc, and J. Courtial, "Dr tim: Ray-tracer tim, with additional specialist scientific capabilities," Comput. Phys. Commun. **185**(3), 1027–1037 (2014).

37. "TIM: A raytracer for forbidden optics," http://sourceforge.net/projects/timray/.